

Creep and creep recovery under stress-controlled subloop loading in TiNi shape memory alloy

K. TAKEDA¹⁾, R. MATSUI¹⁾, H. TOBUSHI¹⁾, E. A. PIECZYSKA²⁾

¹⁾*Department of Mechanical Engineering
Aichi Institute of Technology
1247 Yachigusa, Yakusa-cho, Toyota 470-0392, Japan
e-mail: tobushi@aitech.ac.jp*

²⁾*Institute of Fundamental Technological Research
Polish Academy of Sciences
Pawinskiego 5B
02-106 Warsaw, Poland
e-mail: epiecz@ippt.gov.pl*

IF A SHAPE MEMORY ALLOY (SMA) is subjected to the subloop loading under the stress-controlled condition, creep and creep recovery can appear based on the martensitic transformation. In the design of SMA elements, these deformation properties are important since the deflection of SMA elements can change under constant load. The conditions for the progress of the martensitic transformation are discussed based on the kinetics of the martensitic transformation for the SMA. The creep deformation properties are investigated experimentally for TiNi SMA. The creep strain rate increases in proportion to the martensitic transformation strain; the creep recovery strain rate increases in proportion to the reverse transformation strain.

Key words: shape memory alloy, superelasticity, subloop, transformation band, creep, creep recovery, strain rate, local deformation.

Copyright © 2013 by IPPT PAN

1. Introduction

SHAPE MEMORY ALLOYS (SMAs) are high functional materials characterized by the thermomechanical properties of shape memory effect and superelasticity (SE). Since properties like these are highly conducive to the functions of smart materials, their applications have attracted worldwide attention [1–3]. However, in order for SMAs to be applied effectively in the design of shape memory elements, the thermomechanical properties of the material have to be taken into account. The functional properties of an SMA appear based on the martensitic transformation (MT), and since the MT is sensitive to variations in temperature and stress and to their hysteresis, the deformation properties due to the MT are complex [4, 5]. Up to now, research in this area has

been mainly concerned with a full loop (or perfect loop) of the MT completion under a certain loading condition. But in practical applications, temperature and stress are likely to vary in various ranges. If SMA elements are subjected to loads with a subloop (or partial loop, internal loop), in which the loading condition of temperature or stress varies in an incomplete MT range, the conditions for the start and finish of the MT as in a full loop are not satisfied. That is to say, the conditions for the progress of the MT will therefore change depending on the previous hysteresis of temperature and stress [6–9]. An example of this would be a case in which an SMA element accomplishes a two-way movement depending on an MT of cooling and a reverse MT of heating, both under constant stress. In a full loop description, the SMA element undergoes an amount of deformation corresponding to the maximum stress-induced martensitic transformation (SIMT) strain. However, in the case of a subloop, the SMA element does not complete the whole of this stroke. Similarly, since the recovery stress which occurs in an SMA element subjected to heating and cooling under a constant strain will depend on the hysteresis of the temperature, the actual variation in the recovery stress for a given subloop will be smaller than that obtained in a full loop. It can be recognized from this that the subloop deformation behaviour of an SMA is of great importance for an accurate evaluation of the functional properties of SMA elements and for the design of such elements in practical applications. In the previous paper, the basic behavior of transformation-induced creep and creep recovery of SMA under one stress rate for one stress-holding start strain was investigated [10].

The present study investigates the SE deformation properties of TiNi alloy, the most widely used SMA in practical applications. In particular, the characteristics of creep and creep recovery deformation in the stress plateau region under constant stress which appears in the stress-controlled subloop loading are investigated. Variations in the SIMT bands during deformation are observed using a microscope, and a thermograph is used to identify the temperature distributions on the surface of the tape specimen. The influence of stress-holding start strain on creep and creep recovery behaviors is discussed in terms of the local deformations due to the SIMT. Both the creep and creep recovery strain rates increase in proportion to the transformation strain.

2. Conditions for progress of creep and creep recovery

2.1. Conditions of creep behavior in subloop loading

Let us discuss the conditions for strain to increase or decrease under constant stress in the subloop loading or unloading. The transformation kinetics for the

MT in SMAs proposed by TANAKA *et al.* is expressed as follows [4, 11]:

$$(2.1) \quad \frac{\dot{z}}{1-z} = b_M C_M \dot{T} - b_M \dot{\sigma} \geq 0$$

and for the reverse transformation

$$(2.2) \quad -\frac{\dot{z}}{z} = b_A C_A \dot{T} - b_A \dot{\sigma} \geq 0,$$

where σ , T and z represent the stress, temperature and the volume fraction of the martensitic phase (M-phase), respectively. The volume fraction of the parent phase or austenitic phase (A-phase) is $1 - z$. An overdot denotes the time derivative. The material parameters b_M , C_M , b_A and C_A are determined from the experiments.

The conditions for start and finish of the MT are expressed by the following equations, respectively:

$$(2.3) \quad \sigma = C_M(T - M_s),$$

$$(2.4) \quad \sigma = C_M(T - M_f).$$

The conditions for the reverse transformation are as follows, respectively:

$$(2.5) \quad \sigma = C_A(T - A_s),$$

$$(2.6) \quad \sigma = C_A(T - A_f).$$

The parameters M_s , M_f , A_s and A_f denote the start and finish temperatures for the MT and the reverse transformation under no load, respectively.

From Eq. (2.1), since $b_M < 0$, the condition for progress of the MT becomes as follows:

$$(2.7) \quad \begin{aligned} \frac{d\sigma}{dT} &\geq C_M: && \text{for } dT > 0, \\ \frac{d\sigma}{dT} &\leq C_M: && \text{for } dT < 0. \end{aligned}$$

From Eq. (2.2), since $b_A > 0$, the condition for progress of the reverse transformation becomes as follows:

$$(2.8) \quad \begin{aligned} \frac{d\sigma}{dT} &\leq C_A: && \text{for } dT > 0, \\ \frac{d\sigma}{dT} &\geq C_A: && \text{for } dT < 0. \end{aligned}$$

The conditions for progress of the phase transformation in the subloop loading during the phase transformation are shown in the stress-temperature phase

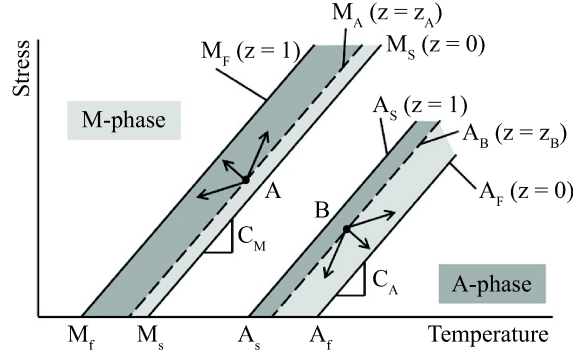


FIG. 1. Conditions for progress of the MT and the reverse transformation in the subloop loadings on the stress-temperature phase diagram.

diagram in Fig. 1. In Fig. 1, M_S ($z = 0$) and M_F ($z = 1$) denote the MT start and finish lines with a slope of C_M , respectively, and A_S ($z = 1$) and A_F ($z = 0$) denote the reverse transformation start and finish lines with a slope of C_A , respectively. Points A and B in Fig. 1, respectively, represent the state of progress of the MT and the reverse transformation and the volume fractions of the M-phase at each point are z_A and z_B . The dashed lines M_A and A_B denote the states with the volume fractions z_A and z_B , respectively. The conditions described by Eqs. (2.7) and (2.8) for progress of the phase transformation from the points A and B mean that stress and temperature vary in the directions shown by the arrows in Fig. 1.

If temperature decreases under constant stress from the point A , the MT progresses. In this case, strain increases due to the MT under constant stress like normal creep deformation. If temperature increases under constant stress from the point B , the reverse transformation progresses. In this case, strain decreases due to the reverse transformation under constant stress like normal creep recovery.

2.2. Thermomechanical paths in stress-controlled subloop loading

The stress-strain diagrams for creep and creep recovery under stress-controlled subloop loading are schematically shown by the continuous line and that for constant strain rate by the dashed line in Fig. 2. The corresponding stress-temperature paths for creep and creep recovery and for constant strain rate are shown in Fig. 3.

In the case of the SE deformation under constant strain rate, the SIMT starts at the point A during loading and the reverse transformation at the point C during unloading. The slope of the lines AB and CD in the stress-strain diagram

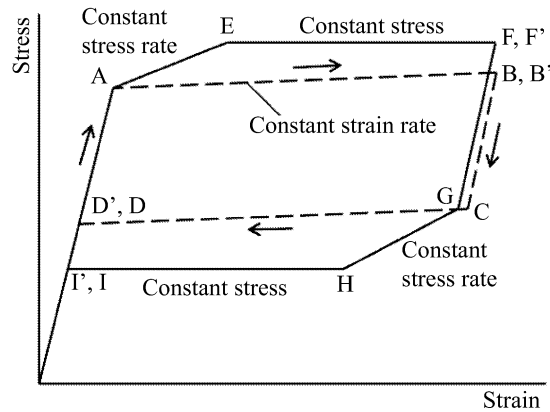


FIG. 2. Stress-strain diagrams for creep and creep recovery under stress-controlled subloop loading and for constant strain rate (AE, F'GH – constant stress rate, EFF', HII' – constant stress, AB, B'CD – constant strain rate).

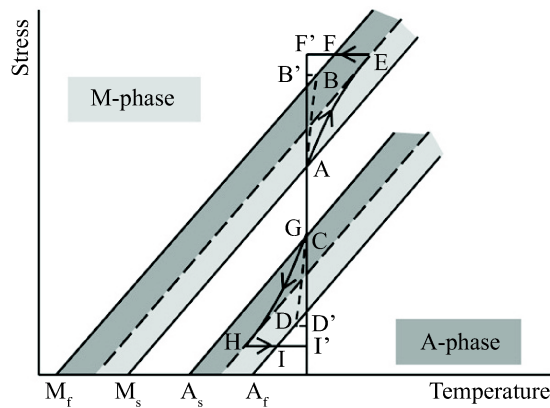


FIG. 3. Stress-temperature paths for creep and creep recovery under stress-controlled subloop loading and for constant strain rate (AE, F'GH – constant stress rate, EFF', HII' – constant stress, AB, B'CD – constant strain rate).

is gentle under low strain rate and steep under high strain rate [12–16]. In the case of constant stress rate, the slope of the lines AE and GH in the stress-strain diagram is steep in proportion to stress rate [17]. Temperature increases due to the SIMT in the process AE and decreases due to the reverse transformation in the process GH. If stress is kept constant at the point E, temperature decreases, resulting in an increase in creep strain due to the SIMT from the point E to the point F. If stress is kept constant at the point H, temperature increases, resulting in a decrease in creep recovery strain due to the reverse transformation from the point H to the point I. These properties will be discussed based on the experimental results in the following sections.

3. Experimental method

3.1. Materials and specimens

The material used in the tests was a TiNi alloy containing Ti-50.95 at % Ni. The specimens were in the form of a polycrystalline tape of this material produced by Furukawa Techno Material Co., Ltd. The transformation temperatures R_s , R_f , A_s and A_f of the material obtained from the differential scanning calorimeter (DSC) test were 279 K, 245 K, 254 K and 281 K, respectively. This material shows SE at room temperature. The thickness and the width of the tape were uniform, at 0.377 mm and 9.81 mm, respectively. The final cold-rolling rate was 25% and the heat-treatment temperature was 803 K for 1 min. The specimen used in the test was of gage length, 100 mm, where “gage length” (GL) means the distance between the two securing grips.

The surface of the specimen used to observe the SIMT bands was mirror-like, finished with a 2000 Grade emery paper. The surface used to detect the temperature distributions by means of infrared thermography was covered with a thin black layer of carbon powder.

3.2. Experimental apparatus

The testing apparatus for SMA characteristics appearing in the tension test consisted of a tension machine and a heating-cooling device. A motion analysis microscope (VW-6000 series by Keyence Co. Ltd) was used for the observation of the SIMT bands on the surface of the specimen and an infrared thermography device (NEC Avio Thermo Tracer H2600) was used for the detection of heating or cooling effects due to exothermic or endothermic reactions to the SIMT.

3.3. Experimental procedure

The stress-controlled subloop tension test for creep and creep recovery was carried out in air at room temperature. The test was carried out as follows. Stress loading was applied at a constant rate $d\sigma/dt = 5$ MPa/s up to a strain of ε_1 in the upper stress plateau, and stress was then kept constant while the creep deformation was observed. After reaching, at the maximum, strain ε_m due to the creep deformation, stress was removed at the constant rate $d\sigma/dt = -5$ MPa/s down to a strain of ε_3 in the lower stress plateau during unloading, and stress was then kept constant while the creep recovery behavior was observed. During the test, the SIMT band characteristics and the temperature distributions on the surface of the specimen were measured continuously.

4. Transformation-induced creep and creep recovery

4.1. Strain behavior under constant stress in subloop loading

Figure 4 shows the stress-strain curve obtained from the stress-controlled subloop tension test for creep and creep recovery in which stress loading was applied under a constant stress rate of 5 MPa/s up to a strain ε_1 of 2% in the upper stress plateau during loading, followed by a constant stress till a stop of creep strain, and then stress was removed under a constant stress rate of -5 MP/s down to a strain ε_3 of 6.41% with a decrease in strain of 1.5% from the maximum strain ε_m in the lower stress plateau during unloading, followed by a constant stress till a stop of creep recovery strain. In Fig. 4, the SIMT starts at a strain ε_{MS} of 1.3% (point S_M) in the loading process, under a constant stress rate. If stress is controlled so as to remain constant at its level for strain $\varepsilon_1 = 2\%$ (point H_1), it initially fluctuates slightly before setting down to a constant 508 MPa at a strain of 3.5% (point C_1). This fluctuation occurs due to the fact that the tension test machine can not control the stress constant precisely just after the change in stress rate. Strain thereafter continues to increase from point C_1 to 7.91% (point F_M). This phenomenon of strain increase under constant stress is similar to what is found with normal creep deformation. The explanation in this case would be that the SIMT causes the temperature to increase during loading up to a strain of 2%, after which it decreases under a constant stress. Conditions are therefore satisfied for the SIMT to progress as discussed in Figs. 2 and 3 (point E to F) in Section 2, and strain increases.

In the unloading process, strain decreases elastically from point H_2 to a strain ε_{AS} of 6.9% (point S_A) at which the reverse transformation starts. If stress is

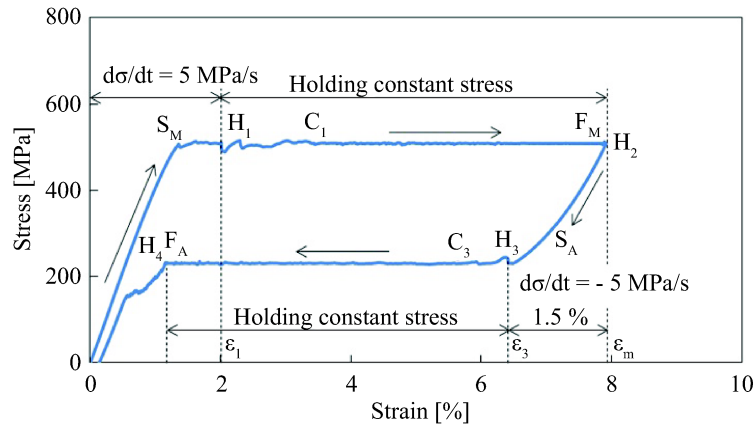


FIG. 4. Stress-strain curve under a stress rate of 5 MPa/s followed by holding constant stress at 508 MPa from a strain of $\varepsilon_1 = 2\%$ (point H_1) during loading and holding constant stress at 231 MPa from a strain of ε_3 (point H_3) following a decrease in strain of 1.5% from the maximum strain ε_m (point H_2) under a stress rate of -5 MPa/s during unloading.

controlled so as to remain constant at its level for strain $\varepsilon_3 = 6.41\%$ (point H_3), it initially fluctuates slightly before settling down to a constant 231 MPa at a strain of 5.8% (point C_3). Strain then continues to decrease to 1.14% (point F_A). This phenomenon of strain decrease under constant stress is similar to what is found with normal creep recovery deformation. The explanation in this case would be that the reverse transformation causes the temperature to decrease during unloading down to point H_3 , after which it increases under a constant stress. Conditions are therefore satisfied for the reverse transformation to progress as discussed in Figs. 2 and 3 (point H to I) in Section 2, and strain decreases.

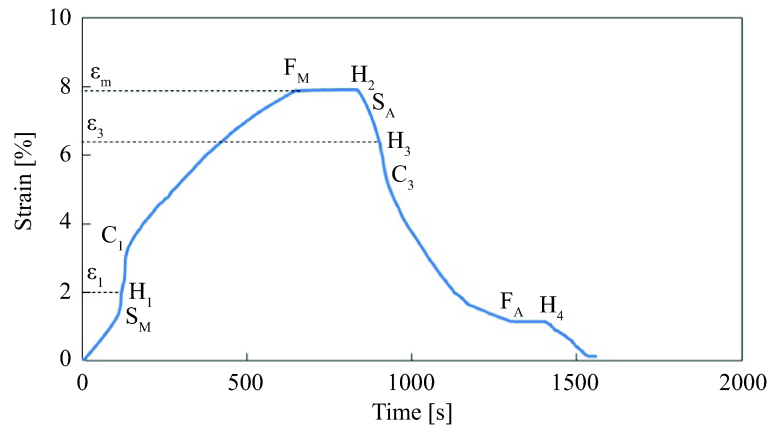


FIG. 5. Variation in strain with time in the creep and creep recovery test under a stress rate of 5 MPa/s followed by holding constant stress from a strain of $\varepsilon_1 = 2\%$ (point H_1) during loading and holding constant stress from a strain of ε_3 (point H_3) following a decrease in strain of 1.5% from the maximum strain ε_m (point H_2) under a stress rate of -5 MPa/s during unloading.

The relationship between strain and time is shown in Fig. 5. As can be seen in Figs. 4 and 5, the rate of increase in strain rises sharply at the level of 1.3 % (point S_M), following the start of the SIMT. Stress fluctuates slightly between strain levels $\varepsilon_1 = 2\%$ (point H_1) and 3.5% (point C_1) while strain increases rapidly. After a strain of 3.5% is reached, stress settles down to be constant and strain increases at an almost constant rate of $8.48 \times 10^{-5} \text{ s}^{-1}$. Strain goes on increasing to $\varepsilon_m = 7.91\%$ before finally becoming constant (points F_M-H_2).

In the unloading process from point H_2 , the rate of decrease in strain rises sharply following the start of the reverse transformation at point S_A . Stress fluctuates slightly between point H_3 and point C_3 while strain decreases rapidly. After point C_3 is reached, stress settles down to be constant and strain decreases at an almost constant rate of $-1.52 \times 10^{-4} \text{ s}^{-1}$. Strain goes on decreasing gradually to a strain of 1.14% before finally becoming constant (point F_A-H_4).

4.2. Progress of creep and creep recovery

Figure 6 shows photographs of specimen surface at various strains ε taken by a motion analysis microscope in the stress-controlled subloop tension test for creep and creep recovery. As can be observed from the series of images in Fig. 6, the bands left by the SIMT (SIMT bands), similar to Lüders bands but at a certain angle of inclination, appear first at both ends and then spread toward the center as stress is kept constant from a strain of $\varepsilon_1 = 2\%$. Once the whole surface has been transformed to the M-phase at a strain of $\varepsilon_m = 7.91\%$, the strain stops growing. The inclined angle of the SIMT bands in the central part of the specimen is 42° which is close to the direction of maximum shearing stress of 45° suggested by HUANG [18].

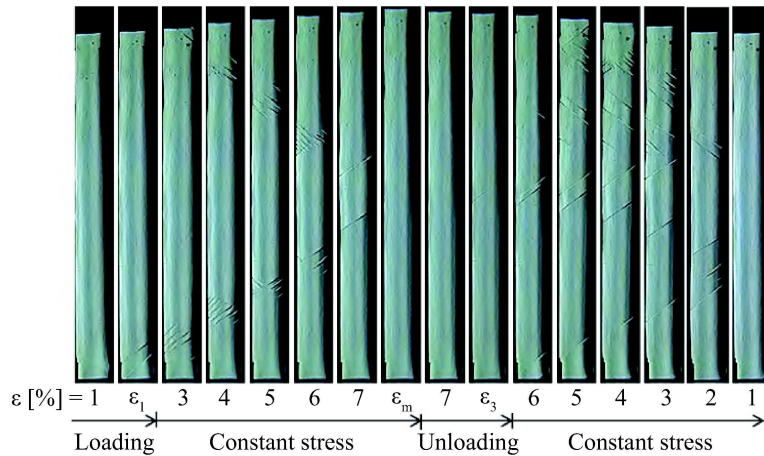


FIG. 6. Photographs of specimen surface at various strains ε under a stress rate of 5 MPa/s followed by holding constant stress from a strain of $\varepsilon_1 = 2\%$ during loading and holding constant stress from a strain of ε_3 following a decrease in strain of 1.5% from the maximum strain ε_m under a stress rate of -5 MPa/s during unloading.

In the unloading process, the reverse transformation band does not appear in the early stage of unloading since stress decreases due to the elastic deformation of the M-phase. If stress is kept constant at $\varepsilon_3 = 6.41\%$, the reverse transformation bands, after first appearing at the two ends and the central part, spread from the boundaries to the whole surface.

Figure 7 shows the thermograms of the temperature distributions on the surface of the specimen at various strains ε obtained by the infrared thermography in the subloop tension test. As it can be seen from the temperature distributions, the SIMT process, due to the exothermic reaction, first appears at the two ends during loading and then spreads toward the center. If the stress is kept constant at the level reached for a strain $\varepsilon_1 = 2\%$, the SIMT bands spread due to a decrease in temperature. Transformation heat is generated at each new

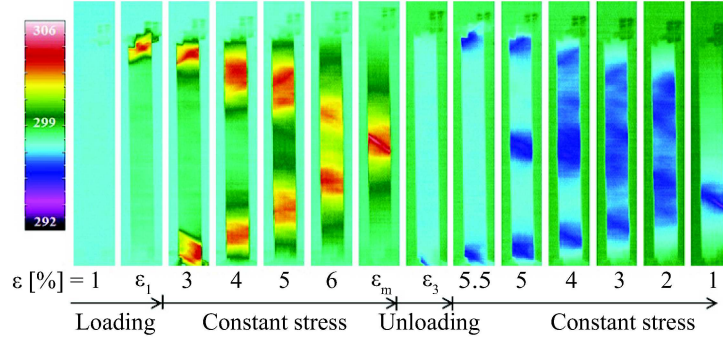


FIG. 7. Thermograms of temperature distribution on the specimen surface under a stress rate of 5 MPa/s followed by holding constant stress from a strain of $\varepsilon_1 = 2\%$ during loading and holding constant stress from a strain of ε_3 following a decrease in strain of 1.5% from the maximum strain ε_m under a stress rate of -5 MPa/s during unloading.

point of advance in the SIMT process, which leads to a chain reaction in the SIMT, resulting in creep deformation. The creep deformation corresponds to the thermomechanical path E to F in Fig. 3. When the SIMT bands combine at the maximum strain $\varepsilon_m = 7.38\%$ in the center, temperature increases a little higher than that during spreading of the SIMT bands.

In the unloading process, the reverse transformation appears first, due to endothermic reaction, at the two ends. If stress is kept constant from a strain $\varepsilon_3 = 5.88\%$, the reverse transformation bands spread due to an increase in temperature from both ends and the central part, resulting in creep recovery. The creep recovery deformation corresponds to the thermomechanical path H to I in Fig. 3.

4.3. Influence of stress-holding start strain on creep behavior

Figure 8 shows the relationship between strain and time obtained from the creep and creep recovery test in which stress loading was applied under a constant stress rate of 5 MPa/s up to various stress-holding start strains $\varepsilon_1 = 2\%$, 3% and 4% (point H_1), followed by a constant stress till a stop of creep strain (point F_M) at the maximum strain ε_m , and then stress was removed under a constant stress rate of -5 MPa/s down to the stress-holding start strain $\varepsilon_3 = \varepsilon_m - 1.5\%$ (point H_3), followed by a constant stress till a stop of creep recovery strain (point F_A). As can be seen in Fig. 8, the overall strain behaviors are similar to the ones observed in Fig. 5. If the stress-holding start strain ε_1 is large, the strain rate under constant stress is high and the maximum strain ε_m is large. The average creep strain rates $\dot{\varepsilon}_c$ under constant stress (from point C_1 to point F_M) for $\varepsilon_1 = 2\%$, 3% and 4% are $8.41 \times 10^{-5} \text{ s}^{-1}$, $1.13 \times 10^{-4} \text{ s}^{-1}$ and

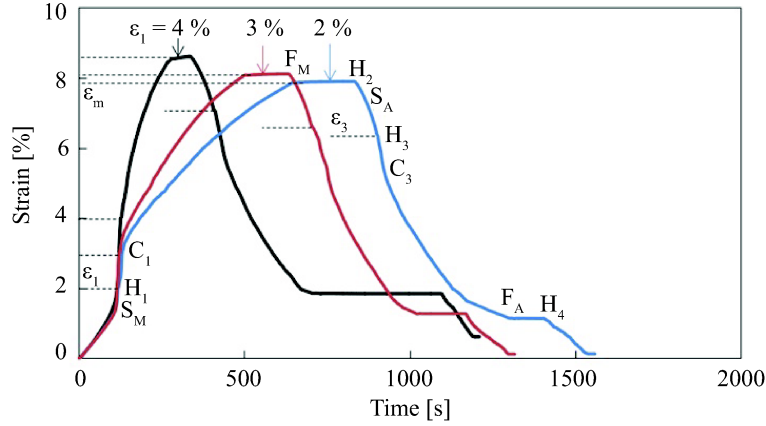


FIG. 8. Variations in strain with time in the creep and creep recovery test under a stress rate of 5 MPa/s followed by holding constant stress from various strains ϵ_1 (point H_1) of 2%, 3% and 4% during loading and holding constant stress from a strain of ϵ_3 (point H_3) following a decrease in strain of 1.5% from the maximum strain ϵ_m (point H_2) under a stress rate of -5 MPa/s during unloading.

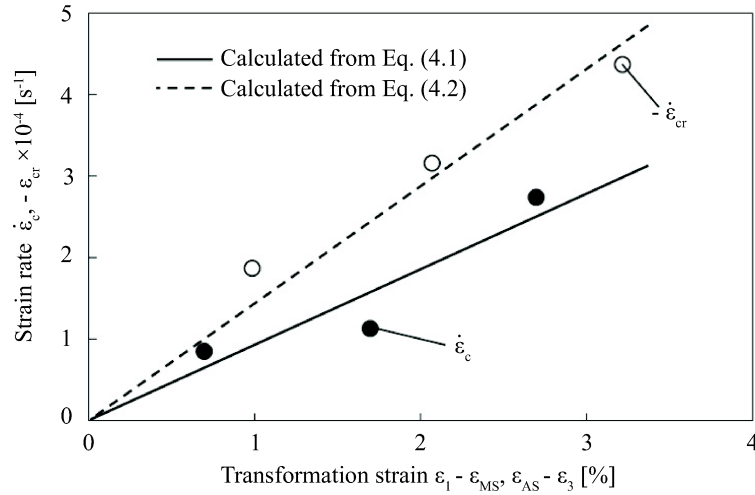


FIG. 9. Relationships between creep strain rate $\dot{\epsilon}_c$ and MT strain $\epsilon_1 - \epsilon_{MS}$, and creep recovery strain rate $-\dot{\epsilon}_{cr}$ and reverse transformation strain $\epsilon_{AS} - \epsilon_3$.

$2.74 \times 10^{-4} \text{ s}^{-1}$, respectively. The relationship between the creep strain rate $\dot{\epsilon}_c$ and the MT strain $\epsilon_1 - \epsilon_{MS}$ is shown in Fig. 9. The creep strain rate $\dot{\epsilon}_c$ can be approximated by the following equation:

$$(4.1) \quad \dot{\epsilon}_c = a(\epsilon_1 - \epsilon_{MS}),$$

where $\epsilon_{MS} = 1.3\%$ denotes the SIMT start strain and the coefficient

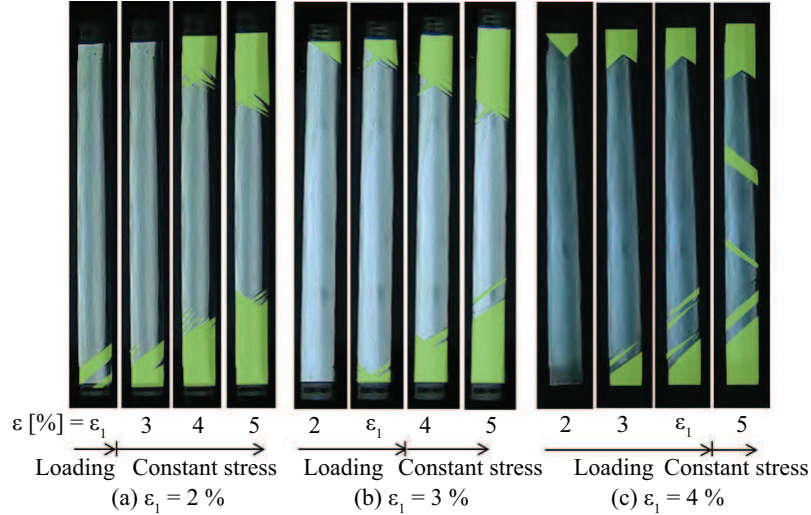


FIG. 10. Photographs of specimen surface at various strains ε under a stress rate of 5 MPa/s followed by holding constant stress from various stress-holding start strains ε_1 of 2%, 3% and 4% during loading.

$a = 9.3 \times 10^{-3} \text{ s}^{-1}$. As can be seen in Fig. 8, the creep recovery strain behaviors with time under constant stress (from point H_3 to point F_A) are almost the same in all cases. The creep strain rate may depend on the hysteresis of stress and temperature. This point is the future subject.

Figure 10 shows photographs of specimen surface at various strains ε during loading in the creep and creep recovery test for various stress-holding start strains $\varepsilon_1 = 2\%$, 3% and 4% taken by a motion analysis microscope. In Fig. 10, the SIMT bands have been enhanced with green tinting. This is because the propagation patterns of these bands although obvious enough to naked-eye observation, do not show up well in monochrome photographs. As can be observed from the series of images, the SIMT bands appear first at both ends and then spread toward the center in the case of small stress-holding start strain ε_1 . In the case of large stress-holding start strain ε_1 , the SIMT bands appear not only at both ends but also in various central parts.

Figure 11 shows thermograms of the temperature distribution on the surface of the specimen at various strains ε during loading for various stress-holding start strains ε_1 observed by the infrared thermography. In the case of $\varepsilon_1 = 2\%$, the SIMT bands appear at both ends and then spread toward the center with slight increase in temperature. In the case of $\varepsilon_1 = 3\%$, the SIMT bands appear at both ends and central part with high increase in temperature. In the case of $\varepsilon_1 = 4\%$, the SIMT bands appear at both ends and various parts with high increase in temperature and wide high-temperature area, resulting in an increase

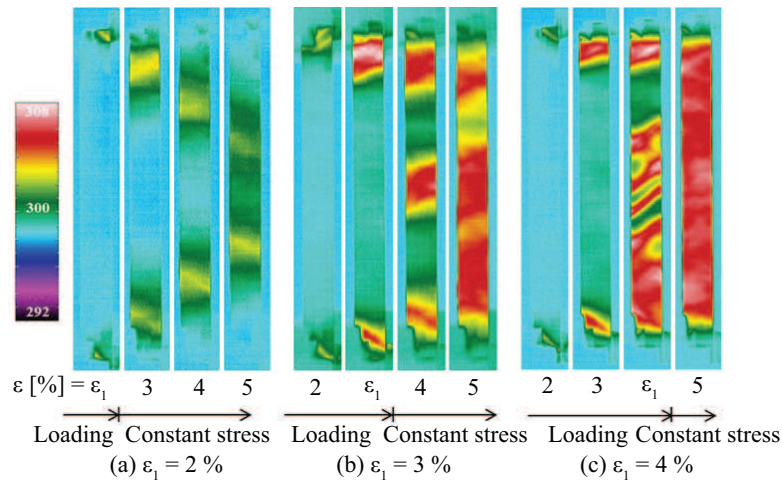


FIG. 11. Thermograms of temperature distribution on the specimen surface under a stress rate of 5 MPa/s followed by holding constant stress from various stress-holding start strains ϵ_1 of 2%, 3% and 4% during loading.

in creep strain rate as observed in Fig. 8. If ϵ_1 is large, temperature rise is large during the path from A to E in Fig. 3, resulting in high creep strain rate during the path from E to F.

4.4. Influence of stress-holding start strain on creep recovery

Figure 12 shows the relationship between strain and time during unloading obtained from the creep and creep recovery test in which stress was removed from

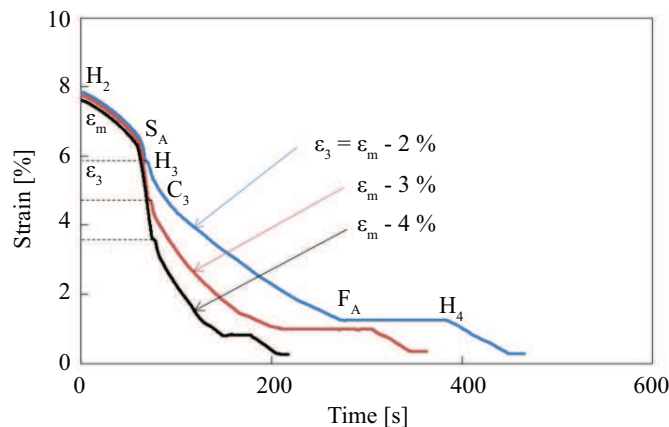


FIG. 12. Variations in strain with time in the creep recovery test under a stress rate of 5 MPa/s followed by holding constant stress from various stress-holding start strains ϵ_3 (point H_3) following a decrease in strain of 2%, 3% and 4% from the maximum strain ϵ_m (point H_2) under a stress rate of -5 MPa/s during unloading.

the maximum strain ε_m (point H_2) under a constant stress rate of -5 MPa/s down to various stress-holding start strains $\varepsilon_3 = \varepsilon_m - 2\%$, $\varepsilon_m - 3\%$ and $\varepsilon_m - 4\%$ (point H_3), followed by a constant stress till a stop of creep recovery strain (point F_A). If the amount of strain removal $\varepsilon_m - \varepsilon_3$ from the maximum strain is large, the strain rate under constant stress is high. The average creep recovery strain rates $\dot{\varepsilon}_{cr}$ under constant stress (from point C_3 to point F_A) for $\varepsilon_3 = \varepsilon_m - 2\%$, $\varepsilon_m - 3\%$ and $\varepsilon_m - 4\%$ are $-1.87 \times 10^{-4} \text{ s}^{-1}$, $-3.16 \times 10^{-4} \text{ s}^{-1}$ and $-4.37 \times 10^{-4} \text{ s}^{-1}$, respectively. The relationship between the creep recovery strain rate $-\dot{\varepsilon}_{cr}$ and the reverse transformation strain $\varepsilon_{AS} - \varepsilon_3$ is shown in Fig. 9. The creep recovery strain rate $\dot{\varepsilon}_{cr}$ can be roughly approximated by the following equation:

$$(4.2) \quad \dot{\varepsilon}_{cr} = b(\varepsilon_3 - \varepsilon_{AS}),$$

where $\varepsilon_{AS} = 6.9 \%$ denotes the reverse transformation start strain and the coefficient $b = 1.4 \times 10^{-2} \text{ s}^{-1}$. The creep recovery strain rate may depend on the hysteresis of stress and temperature. This point is the future subject.

5. Conclusions

The creep and creep recovery under the stress-controlled subloop loading in TiNi SMA tape were investigated based on evidence of local temperature variation as measured by infrared thermography and on the SIMT band that appeared on the surface and was observed by a motion analysis microscope during tension tests. The results obtained can be summarized as follows:

- (1) If stress is kept constant at the upper stress plateau after loading up to the stress-holding start strain ε_1 under a constant stress rate, creep deformation occurs due to the spread of the SIMT process. The creep strain rate under constant stress increases in proportion to the MT strain $\varepsilon_1 - \varepsilon_{MS}$ based on temperature increase due to the exothermic SIMT up to the strain ε_1 .
- (2) If stress is kept constant at the lower stress plateau after unloading down to the stress-holding start strain ε_3 from the maximum strain under a constant stress rate, creep recovery deformation occurs due to the reverse transformation. The relationship between the creep recovery strain rate under constant stress and the reverse transformation strain $\varepsilon_3 - \varepsilon_{AS}$ can be roughly approximated by a linear relationship.
- (3) In the design of SMA elements, it is important to take account of the creep and creep recovery since the deflection of SMA elements can vary under constant load even if temperature is kept constant around SMA elements.

Acknowledgements

The experimental work was carried out with the assistance of students of Aichi Institute of Technology, to whom the authors wish to express their gratitude. The authors wish to express their gratefulness to the Joint Research Project between two countries supported by Polish Academy of Sciences and Japan Society for Promotion of Science (JSPS), the Basic Research (C) of a Grant-in-Aid of Scientific Research supported by JSPS and The Naito Research Grant for their financial supports. The research was also partly supported by the National Science Centre of Poland NCN under Grant No. 2011/01/M/ST8/07754.

References

1. H. FUNAKUBO, *Shape Memory Alloys*, Gordon and Breach Science Pub., New York, U.S.A., 1987.
2. K. OTSUKA, C.M. WAYMAN, *Shape Memory Materials*, Cambridge University Press, Cambridge, U.K., 1998.
3. C. CISMASIU, *Shape Memory Alloys*, Sciyo, Rijeka, Croatia, 2010.
4. K. TANAKA, S. KOBAYASHI, Y. SATO, *Thermomechanics of transformation pseudoelasticity and shape memory effect in alloys*, *Inter. J. Plasticity*, **2**, 59–72, 1986.
5. B. RANIECKI, C. LEXCELLENT, K. TANAKA, *Thermodynamic models of pseudoelastic behaviour of shape memory alloys*, *Arch. Mech.*, **44**, 3, 261–284, 1992.
6. K. TANAKA, F. NISHIMURA, H. TOBUSHI, *Phenomenological analysis on subloop in shape memory alloys due to incomplete transformations*, *J. Intell. Mater. Syst. Struct.*, **5**, 487–493, 1994.
7. P.H. LIN, H. TOBUSHI, K. TANAKA, T. HATTORI, M. MAKITA, *Pseudoelastic behaviour of TiNi shape memory alloy subjected to strain variations*, *J. Intell. Mater. Syst. Struct.*, **5**, 694–701, 1994.
8. K. TANAKA, F. NISHIMURA, T. HAYASHI, H. TOBUSHI, C. LEXCELLENT, *Phenomenological analysis on subloops and cyclic behavior in shape memory alloys under mechanical and/or thermal loads*, *Mech. Mater.*, **19**, 281–292, 1995.
9. E.A. PIECZYSKA, H. TOBUSHI, W.K. NOWACKI, S.P. GADAJ, T. SAKURAGI, *Subloop deformation behavior of TiNi shape memory alloy subjected to stress-controlled loadings*, *Mater. Trans.*, **48**, 2679–2686, 2007.
10. K. TAKEDA, H. TOBUSHI, E.A. PIECZYSKA, *Transformation-induced creep and creep recovery of shape memory alloy*, *Materials*, **5**, 909–921, doi: 10.3390/ma5050909, 2012.
11. K. TANAKA, *A thermomechanical sketch of shape memory effect: one-dimensional tensile behavior*, *Res. Mechanica*, **18**, 251–263, 1986.
12. E.A. PIECZYSKA, H. TOBUSHI, S.P. GADAJ, W.K. NOWACKI, *Superelastic deformation behaviors based on phase transformation bands in TiNi shape memory alloy*, *Mater. Trans.*, **47**, 670–676, 2006.

13. Y.J. HE, H. YIN, R.H. ZHOU, Q.P. SUN, *Ambient effect on damping peak of NiTi shape memory alloy*, Mater. Lett., **64**, 1483–1486, 2010.
14. J.A. SHAW, S. KYRIAKIDES, *Thermomechanical aspects of NiTi*, J. Mech. Phys. Solids, **43**, 1243–1281, 1995.
15. Y.J. HE, Q.P. SUN, *Rate-dependent domain spacing in a stretched NiTi strip*, Inter. J. Solids Struct., **47**, 2775–2783, 2010.
16. H. TOBUSHI, R. MATSUI, K. TAKEDA, E.A. PIECZYSKA, *Mechanical Properties of Shape Memory Materials. Materials Science and Technologies, Mechanical Engineering Theory and Applications*, NOVA Publishers, New York, 2013.
17. E.A. PIECZYSKA, H. TOBUSHI, K. KULASINSKI, *Development of transformation bands in TiNi SMA for various stress and strain rates studied by a fast and sensitive infrared camera*, Smart Mater. Struct. **22**, 035007 (8 pp.), 2013.
18. W.M. HUANG, *Transformation front in shape memory alloys*, Mater. Sci. Eng., **392**, 121–129, 2005.

Received January 17, 2013; revised version May 16, 2013.
